Proceedings of the 2006 IEEE
International Conference on Mechatronics and Automation
June 25 - 28, 2006, Luoyang, China

Design and Analysis of a Novel Haptic Device*

Yong Zhang+, Minxiu Kong, Lining Sun and Zhijiang Du
Robotics Institute
Harbin Institute of Technology
Harbin, Heilongjiang Province 150080, China
zhangyong212@hit.edu.cn

***Abstract* - A novel 6-DOF parallel haptic device is presented, which is characterized by large workspace, high rigidity, compactness, simple kinematics and easy construction. Its mechanism is composed of three sub-chains, each of which is attached to the base plate through a pin joint and the top plate through a spherical joint. The sub-chain is kinematically equivalent to the pantograph linkage and designed to solve the difficult problem of motor-fitting. The spherical joint belongs to the ball-in-socket type but has much larger workspace than regular ones. The forward and inverse kinematic analyses of the mechnism are performed, and Jacobian matrix is derived. The workspace is analyzed with a new scanning search method of the spherical coordinate searching algorithm, by which the intersections of multi-connected domains are readily obtained.**

Index Terms* - *Haptic devices, parallel mechanisms, spherical joints, kinematics, workspace.

I. INTRODUCTION

Haptic devices are generally operated by human hand contact force to control the motions of slave manipulators or computer graphics, corresponding to the applications of teleoperation and virtual reality respectively. From the perspective of man-machine interaction, a haptic device serves not only as an input device to accept its operator's instructions, but also as an output device to provide feedback force. Consequently, it can give the human a sensation that he/she is maneuvering a mass, or pushing onto a spring or a damper [1]. Various structures have been proposed in the last two decades[11] [12], which can be generally categorized into two types of series structures and parallel structures. Because of the characteristics of large bandwidth, compactness [13], [14], and versatility, parallel structures are more favored than series structures in the area of haptic devices.

A perfect haptic device should have large workspaces, low inertia, high stiffness, low friction, high control bandwidth, simple kinematics and so on. It is, nevertheless, almost impossible to achieve all of them when designing. Owing to that the haptic device will be used in tele-surgery [2], high rigidity, safeness and large workspaces are more emphasized.

Among major mechanism elements, the pantograph linkage or its modifications has been utilized by several research groups as the key part of a sub-chain, three of which constitute their separate haptic devices. Long and Collins [3], [4] and Iwata [5] proposed the first haptic device of this series. The haptic device whose kinematic structure is shown in Fig. 1(a) is composed of three pantograph linkages, each of which is attached to one midpoint of an equilateral base triangle through a passive revolute joint. At the opposite end, each pantograph is connected with one vertex of an equilateral top triangle through a passive three degree-of-freedom ball-in-socket joint. The presentation of this device is of clear theoretical significance, but it has serious disadvantages of small position and orientation workspaces due to the restricted rotation range of spherical joints, and a motor-fitting problem that it is hard to devise a construction for fitting two coaxial motors of a sub-chain. Substituting the fivebar linkage for the pantograph, Woo, Jin and Kwon [6] proposed the fivebar parallel mechanism for solving the motor-fitting problem. This device which is shown in Fig. 1(b), however, still has small workspaces due to spherical joints, and besides, the use of the fivebar linkage brings more complex kinematics. Yoon and Ryu [7] designed another kinematic structure (see Fig. 1(c)) based on the pantograph. It moves the passive revolute joint from the bottom where it connects the pantograph and the base plate to the top where it connects the pantograph and the top plate, so that motors can be fixed to the base plate, and consequently the inertia is reduced. To enlarge the workspace, it also substitutes the RRR-type joint for the ball-in-socket joint. This kind of joint, nonetheless, involves more links and joints, resulting in the decrease in the mechanism stiffness and the increase in the number of error influencing factors.

On the basis of the existing pantograph-type haptic device discussed above, this paper presents the model of a novel haptic device. It is composed of three sub-chains, each of which connects to the base plate through a pin joint and the top plate through a spherical joint. It has the same kinematics as the first pantograph-type haptic device. But the spherical joint and the pantograph are redesigned to obtain much larger workspaces and easier construction, respectively.

II. STRUCTURE AND COMPOSITION

The kinematic structure of the haptic device is shown in Fig. 1(d). It consists of three sub-chains with the same structure, each of which connects to the top plate through a spherical joint and the base plate through a pin joint. The sub-chain is composed of a six-bar ring and inner three bars. It can be readily figured out that the sub-chain has the same kinematics as the pantograph, but it is designed differently and more sophisticatedly for three considerations. First, the two

* This work was supported by the National High-Tech Research and Development Program of China under contract number 2002AA420100.
+ Corresponding author. Tel.: 86-451-86414462-14; fax: 86-451-86414174.

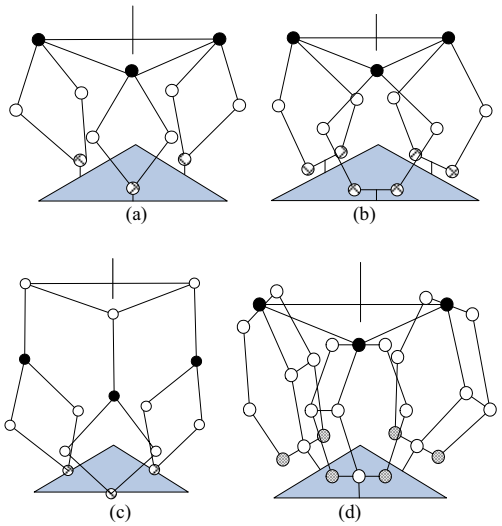

Fig. 1 Kinematic structure of pantograph-type haptic devices. (a) UCI hand controller. (b) KAIST master hand. (c) KJIST haptic device. (d) Proposed mechanism.

motors driving one chain are not fixed coaxially, but are situated inside the closed-chain mechanism to reduce the size of the whole device. Secondly, the chains should be designed spatially to avoid link interference, for that the three inner bars being protruded. The third aspect is that a simple kinematics should be obtained. For one of the three sub-chains, the plane including the axis of the pin joint and perpendicular to the two axes of the motors should include the center point of the ball of the spherical joint.

Another improvement is for the spherical joint. Existing parallel mechanisms using spherical joints have relatively small workspaces because of the rotational limitation of ball-in-socket spherical joints in them. Therefore, some substitute joints with three rotational degrees of freedom have been proposed, such as RRR-type spherical joints. However, due to more links and joints involved, these substitute joints lead to the decrease in the stiffness of the whole mechanisms. To take advantage of the high stiffness of spherical joints, and to avoid the drawback in workspaces, we modified the conventional spherical joints. The improved spherical joint which is shown in Fig. 2 is composed of a ball-bar, a bushing, a shell cover and two ball rings. The root segment of the bar in the ball-bar has smaller diameter than its aft part, resulting in the larger cone angle the joint can achieve. This practice decreases the mechanical strength of the spherical joints and hence the strength of the whole mechanism, but this negative influence can be calculatedly neglected because the load applied by human hands on the mechanism is very low.

For geometric parameters in Fig. 2(b), the angles denoted by s and s+r can be expressed as

$$s = \arctan\frac{d}{h}$$

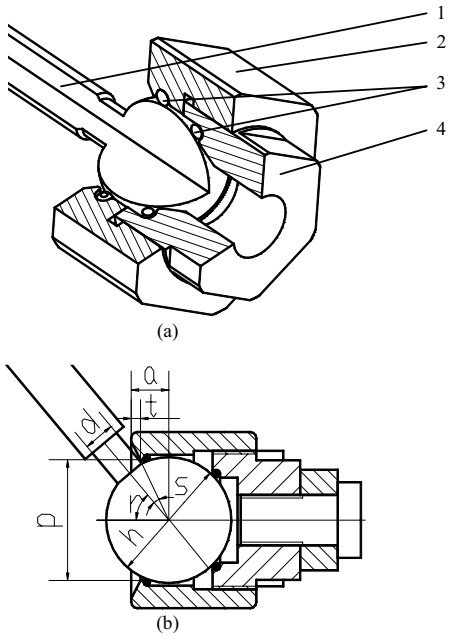

1. ball-bar, 2. bushing, 3. ball rings, 4. shell cover.
Fig. 2 Spherical joint model. (a) Spherical joint details. (b) Spherical joint geometric parameters.

$$s + r = \arctan\frac{p}{2(a-t)}. \quad (1)$$

Thus the angle denoted by r is represented by

$$r = \arctan\frac{p}{2(a-t)} - \arctan\frac{d}{h}. \quad (2)$$

With the diameter d becomes smaller, the angle s decreases, and thus r increases which is half the cone angle of the workspace of the spherical joint.

In a word, if reasonable dimensions are selected for the relevant parameters, the cone angle of this modified spherical joint can achieve 110° without sacrificing other performance indexes. And it will be discussed in Section IV that the workspace of the top plate will no longer enlarge significantly when the cone angle is larger than 110°.

The final CAD design of the device is shown in Fig. 3.

III. Kinematic Analyses

Kinematics analyses have been performed in [3], [8]. The paper rehandles these problems with new approaches.

A. Coordinate System Establishment

In order to analyze the proposed mechanism, kinematic parameters are given in Fig. 4. A base coordinate system {*B-XYZ*} is located at the bottom center of the base plate, where X-axis is in the plane of the base plate and is directed toward the middle of the first sub-chain. The mobile coordinate system {*O-XYZ*} is located at the center of the top plate, where *X*-axis is in the plane of the top plate and is directed toward the first revolute joint. Each sub-chain local coordinate

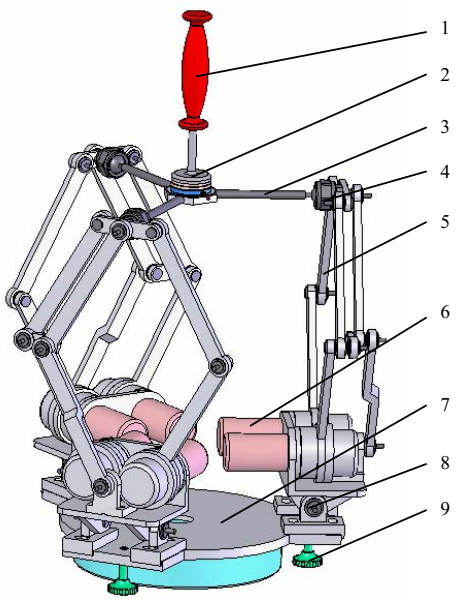

1. joystick, 2. force/torque transducer, 3. top plate, 4. spherical joint, 5. sub-chain, 6. servo motor, 7. base plate, 8. pin joint, 9. balance adjustment.
Fig. 3 Proposed haptic device.

system is located at a passive revolute joint, where the *X*-axis is directed perpendicular to each sub-chain. The axisymmetric positions of the sub-chains on base plate with radius *r* are given by angles δ_i (0, $2\pi/3$ and $4\pi/3$ rads), which specify the rotation angles about *B*-*Z*-axis from *B*-*X*-axis. The connecting bars connecting the base and the sub-chains are denoted by L_1. Lower links of sub-chains are denoted by L_2 and upper links L_3.

It is assumed that the orientation of the top plate in the global coordinate system is obtained through rotation in a certain sequence and with corresponding angles: rotation about *B*-*X*-axis with the angle φ, rotation about *B*-*Y*-axis with the angle θ, and rotation about *B*-*Z*-axis with the angle φ.

$$
\begin{aligned}
{}^{B}Q_O &= R_z(\phi)R_y(\theta)R_x(\varphi) \\
&= \begin{bmatrix} C\phi C\theta & C\phi S\theta S\varphi - S\phi C\varphi & C\phi S\theta C\varphi + S\phi S\varphi & P_X \\ S\phi C\theta & S\phi S\theta S\varphi + C\phi C\varphi & S\phi S\theta C\varphi - C\phi S\varphi & P_Y \\ -S\theta & C\theta S\varphi & C\theta S\varphi & P_Z \\ 0 & 0 & 0 & 1 \end{bmatrix}
\end{aligned} \tag{3}
$$

where, $S\bullet = \sin(\bullet)$ and $C\bullet = \cos(\bullet)$.

B. Inverse Kinematic Analysis

The inverse kinematics involves the computation of the active joint angles $\theta_{1,i}$ and $\theta_{2,i}$ of the *i*th sub-chain as the position and orientation $(x, y, z, \phi, \theta, \varphi)$ of the top plate being given. The position F_i of a spherical joint can be represented by using (4×4) homogeneous matrices in the global reference coordinate system *B*-*XYZ*, and it can be obtained separately

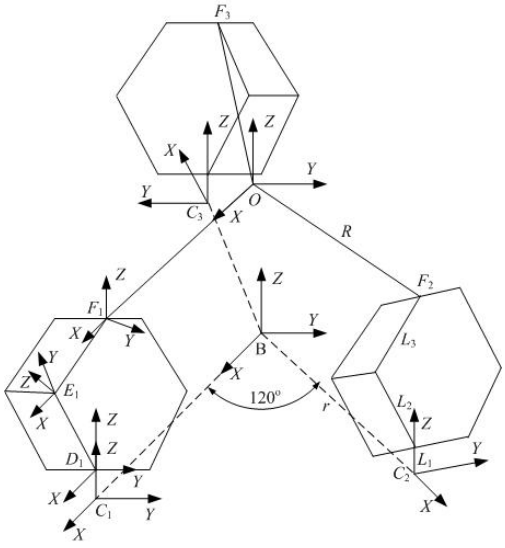

Fig.4 New haptic device kinematic model.

through two paths of ($B \to C_i \to D_i \to F_i$) and($O \to F_i$), and corresponding expressions are:

$$
\begin{aligned}
F_i(x_i, y_i, z_i, 1)^T &= R_z(\delta_i)T(R)R_y(\alpha_i)T_z(L_1)R_x(\theta_{1,i})T_z(L_2) \\
&\quad \times R_x(\theta_{2,i} - \theta_{1,i} - \pi/2)T_z(L_3)[0\ 0\ 0\ 1]^T
\end{aligned} \tag{4}
$$

$$
F_i(x_i, y_i, z_i, 1) = T(x, y, z)R(\phi, \theta, \varphi)R_z(\delta_i)T(r)[0\ 0\ 0\ 1]^T . \tag{5}
$$

The position coordinate of F_i can be directly obtained by solving (5). Inserting F_i into (4) gives a matrix equation with the unknown angles (α_i , $\theta_{1,i}$ and $\theta_{2,i}$) in a closed form. The six active angles are obtained finally.

α_i , $\theta_{1,i}$ and $\theta_{2,i}$ can also be obtained through a geometric method as illustrated in Fig. 5. Transforming $F_i(x_i, y_i, z_i, 1)$ which is obtained by solving (5) into the homogeneous coordinate in the C_i-*XYZ* coordinate system:

$$
{}^{C_i}F_i(x_i', y_i', z_i', 1) = T_X(-R)R_Z(-\delta_i)F_i(x_i, y_i, z_i, 1) . \tag{6}
$$

It can be seen from Fig. 5 that the coordinate of M_i is $(x_i', 0, z_i')$, so α_i is given by

$$
\alpha_i = \arctan\left(\frac{x_i'}{z_i'}\right) \tag{7}
$$

In the triangle $D_iM_iF_i$, β_i is given by

$$
\begin{aligned}
\beta_i &= -\arctan\frac{y_i'}{|M_iD_i|} = -\arctan\frac{y_i'}{|M_iC_i| - |C_iD_i|} \\
&= -\arctan\frac{y_i'}{\sqrt{x_i'^2 + y_i'^2} - d}
\end{aligned} \tag{8}
$$

In the triangle $D_iE_iF_i$, by applying the law of cosine, the angle $\angle F_iD_iE_i$ is given by

$$
\angle F_iD_iE_i = \frac{|F_iD_i|^2 + L_1^2 - L_2^2}{2 \times |F_iD_i| \times L_1} \tag{9}
$$

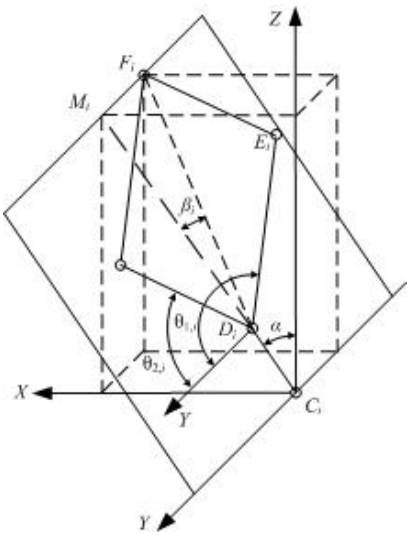

Fig. 5 Geometric solution illustration.

where the length $|F_iD_i|$ is given by

$$|F_iD_i| = \sqrt{|M_iD_i|^2 - y_i^2} \,. \tag{10}$$

Finally, active angles are given by

$$\theta_{1,i} = \frac{\pi}{2} + \beta_i + \angle F_iD_iE_i$$

$$\theta_{2,i} = \frac{\pi}{2} + \beta_i - \angle F_iD_iE_i \,. \tag{11}$$

C. Forward Kinematic Analysis

Forward kinematic analysis determines the position and orientation of the *O-XYZ* coordinate system which are denoted by ($x, y, z, \phi, \theta, \varphi$) with respect to the *B-XYZ* coordinate system given the actuated angles $\theta_{1,i}$ and $\theta_{2,i}$. The first thing to solve forward kinematics is to find the revolute joint angle α_i at C_i point. These three angles can be obtained by the fact that the distance between two of the three points (F_1, F_2 and F_3) is $\sqrt{3}$ times as long as the radius of top plate. The detailed calculating procedure is as follows.

1) The position of the point F_i should be calculated by inserting $\theta_{1,i}$ and $\theta_{2,i}$ into (4).

2) For obtaining the unknown angle α_i, the following three geometric equality conditions are used:

$$|F_1 - F_2| = \sqrt{3}r$$

$$|F_2 - F_3| = \sqrt{3}r$$

$$|F_3 - F_1| = \sqrt{3}r \,. \tag{12}$$

The set of nonlinear equations (12) should be solved for the variable α_i by using the Newton-Raphson's numerical method.

3) F_1, F_2 and F_3 are the vertexes of an equilateral triangular, whose center is the origin of the coordinate system of the top plate.

$$P = \frac{F_1 + F_2 + F_3}{3} \tag{13}$$

The pose of the coordinate system *O-XYZ* can be expressed by the following equations, which give the directions of *X*-axis, *Y*-axis and *Z*-axis, respectively.

$$n = \frac{(F_1 - F_2) + \frac{1}{2}(F_2 - F_3)}{\left|(F_1 - F_2) + \frac{1}{2}(F_2 - F_3)\right|}$$

$$o = \frac{F_3 - F_2}{|F_3 - F_2|}$$

$$a = n \times o \tag{14}$$

Till now, the pose of the top plate is fully determined by ***n***, ***o***, ***a*** and ***P***, which constitute a homogeneous coordinate conversion matrix.

$$D_B^O = \begin{bmatrix} n_x & o_x & a_x & P_x \\ n_y & o_y & a_y & P_y \\ n_z & o_z & a_z & P_z \\ o & 0 & 0 & 1 \end{bmatrix} \tag{15}$$

D. Derivation of Jacobian

The method of mechanism influence coefficient is utilized to derive the Jacobian matrix. The haptic device is capable of being seen as a parallel mechanism composed of three 6-DOF serial mechanisms (*B-C*$_i$*-D*$_i$*-E*$_i$*-F*$_i$*-O*), whose active bars are D_iE_i and E_iF_i. Computing the corresponding Jacobian matrixes yields ($J_1^{-1}, J_2^{-1}, J_3^{-1}$). Actually E_iF_i is a passive bar, so it is necessary to convert the angular rate of E_iF_i denoted by ω_2 to that of D_iH_i ($\omega_2 + \omega_1$), the process of which is illustrated in Fig. 6. The second and the third columns of J_1, J_2 and J_3 are extracted to constitute the Jacobian matrix of the device.

$$J^{-1} = (J_1^{-1}(:,2), J_1^{-1}(:,2) + J_1^{-1}(:,3), J_2^{-1}(:,2),$$
$$J_2^{-1}(:,2) + J_2^{-1}(:,3), J_3^{-1}(:,2)) + J_3^{-1}(:,3)) \tag{16}$$

IV. Workspace Analysis

A. Workspace search method

In order to analyse the workspace, workspace boundaries should be obtained first of all. Several search algorithms have

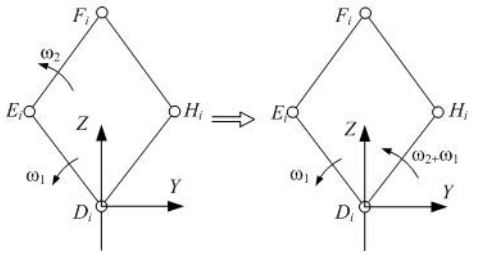

Fig. 6 Rate conversion.

been presented so far, but it is still difficult to obtain the multi-connected domain of some of the intersections. A new search method of the spherical coordinate searching algorism is proposed which is illustrated in Fig. 7, and the procedure is as follows.

1) With regard to an orientation (ϕ,θ,φ), one point in the workspace is selected as the center of sphere.

2) The scanning search in the spherical polar coordinate system is started. The zenith angle denoted by α varies from 0^o to 180^o. The corresponding step length is denoted by $\Delta\alpha$. Assume I=$180^o/\Delta\alpha$, then

$$\alpha(\mathrm{i}) = i \cdot \Delta\alpha \ , \ i = 0,1,2\ldots I. \tag{17}$$

For every zenith angle, β varies from 0° to 360°. The corresponding step length is denoted by $\Delta\beta$. Assume J=$360^o/\Delta\beta$, then

$$\beta(i,j) = j \cdot \Delta\beta, j = 0,1,2\ldots J. \tag{18}$$

For the convenience of description, $\alpha(i)$ is expanded to a 2×2 matrix:

$$\alpha(i,j) = i \cdot \Delta\alpha, i = 0,1,2\ldots I. \tag{19}$$

For every (α, β), the sphere radius r increases from 0 to the infinite. The corresponding step length is denoted by Δr.

$$r(i,j,k) = k \cdot \Delta r, k = 0,1,2\ldots \tag{20}$$

Thus, the coordinate of every discrete spatial point is obtained by:

$$\begin{aligned} x(i,j) &= x0 + r(i,j,k) \cdot \sin\alpha(i,j) \cdot \cos\beta(i,j) \\ y(i,j) &= y0 + r(i,j,k) \cdot \sin\alpha(i,j) \cdot \sin\beta(i,j) \\ z(i,j,k) &= z0 + r(i,j,k) \cdot \sin\alpha(i,j) \cdot \cos\beta(i,j). \end{aligned} \tag{21}$$

For every (α, β, r), the rotation angles of the active joints and the revolute joints can be computed by inserting ($x(i,j), y(i,j), z(i,j,k), \phi,\theta,\varphi$) into the inverse kinematics algorithm. It is can be tested whether the pose is reachable by applying kinematic constraints [10]. k increases gradually until any of the constraints is violated, and the value of k is assigned to K. The value of r corresponding to ($\varphi(i,j)$, $\theta(i,j)$) is obtained by

$$r(i,j) = r(i,j,K), \ z(i,j) = z(i,j,K). \tag{22}$$

The Cartesian coordinate of the boundary point is ($x(i,j), y(i,j), z(i,j)$). By the three-step loop above, all discrete boundary points are obtained.

3) Through a simple algorithm of a two-step loop, every boundary point ($x(i,j), y(i,j), z(i,j)$) is joined to its four peripheral points (($x(i\text{-}1,j)$, $y(i\text{-}1,j)$, $z(i\text{-}1,j)$), ($x(i+1,j)$, $y(i+1,j)$, $z(i+1,j)$), ($x(i,j\text{-}1)$, $y(i,j\text{-}1)$, $z(i,j\text{-}1)$) and ($x(i,j+1)$, $y(i,j+1)$, $z(i,j+1)$) by lines. Thus a visualized mesh boundary is obtained.

4) From Fig. 7, it can be seen that the volume of the workspace is composed of numerous rectangular pyramids (*O-ABCD*). It is assumed, for convenience, that the units of all the angles are changed to radian. The volume of a rectangular pyramid is given by

$$V(i,j) = \frac{1}{3} r(i,j) \cdot r(i,j) \Delta\varphi \cdot r(i,j) \sin\varphi(i,j) \Delta\theta \, . \tag{23}$$

By summing up the volumes of all rectangular pyramids, the workspace volume is obtained:

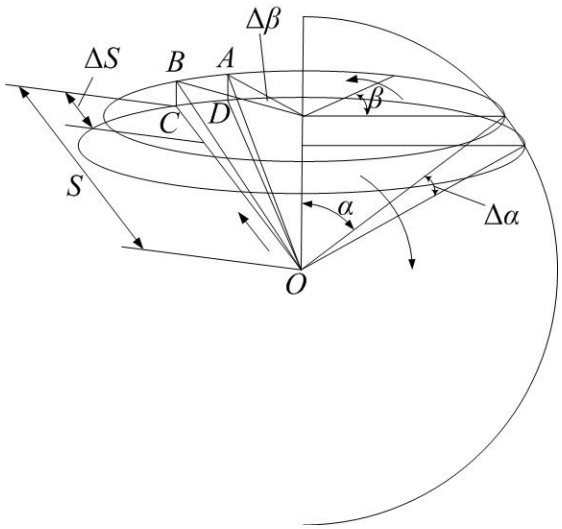

Fig. 7 Spherical coordinate system scanning search method.

$$V = \sum_{i=0:I} \sum_{j=0:J} V(i,j) \, . \tag{24}$$

This method can also be used to search orientation workspace boundaries of 6-DOF parallel mechanisms. Then the boundary point coordinates can be converted to a modified set of Euler angles [9] which can be expressed in a cylinder coordinate system.

B. Workapace analysis of the proposed haptic device

The workspace boundary of the proposed device is determined by the proposed spherical search method. When the orientation of the top plate is ($0^\circ, 0^\circ, 0^\circ$), the position workspace is shown in Fig. 8(a). The corresponding inverted workspace is shown in Fig. 8(b), from which it can be seen that the bottom of the workspace subsides. The horizontal intersections of the upper part of the workspace are circular, while the intersections of the bottom part are six point stars.

As the workspace of the spherical joints increases, the workspace volume of the device increases, which is shown in Fig. 9. It turns out, however, that if half of the cone angle is more than 50°, the enlargement of the workspace is no longer significant. The three curves corresponds to three orientations of the top plate, ($0^\circ, 0^\circ, 0^\circ$), ($4^\circ, 4^\circ, 4^\circ$) and ($6^\circ, 6^\circ, 6^\circ$), respectively.

V. CONCLUSIONS

A novel 6-DOF parallel haptic device has been proposed for the purpose of larger workspace and easier construction. The existing pantograph linkage has been improved for fitting motors and decreasing the device volume. The ball-in-socket spherical joint generally thought as having too much rotational limitation has been utilized, but has been resigned to achieve a much larger cone angle. Inverse kinematics has been performed with the geometric approach. A new universal

scanning search method of the spherical search method has been proposed for readily obtaining the whole workspace boundaries. With this method, the position workspace of the proposed mechanism has been obtained and analyzed.

Currently research on the control system design of the proposed haptic device is no the way.

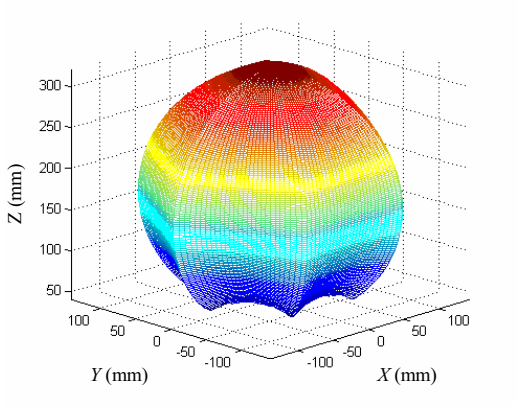

(a)

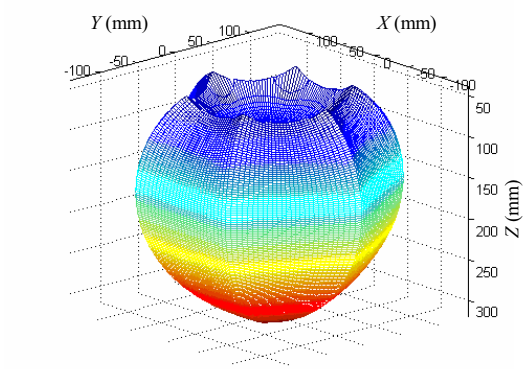

(b)

Fig. 8 Position workspace of the top plate. (a) Workspace. (b) Inverted workspace.

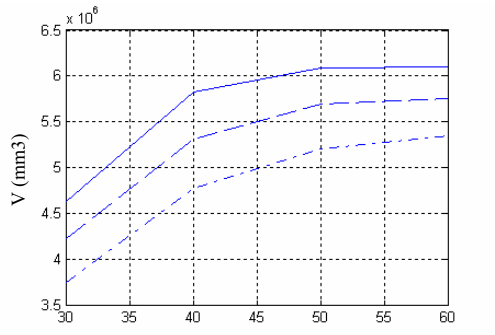

—: orientation (0° , 0° , 0°)

-- : orientation(4° , 4° , 4°)

-—: orientation(6° , 6° , 6°)

Fig. 9 Influence of the spherical joint cone angle on the workspace volume.

ACKNOWLEDGMENT

The authors wish to thank two engineers named Yue Sun and Haisheng Yang for their advice and mechanism fabrication, and to acknowledge out debt to the papers listed below.

REFERENCES

[1] H. Kazerooni and Ming-Guo Her, "The dynamics and control of a haptic interface device," *IEEE Trans. Robotics and Automation*, vol. 10, no. 4, August 1994, pp. 453-464.

[2] Lixin Fu, Zhijiang Du and Lining Sun, "A novel robot-assisted bonesetting system," in *Proc. IEEE Int. Conf. Robotics and Automation*, 2004, pp. 2247-2252.

[3] G. L. Long and C. L. Collins, "A Pantograph linkage parallel platform master hand controller for force-reflection," in *Proc. IEEE Int. Conf. Robotics and Automation*, 1992, pp. 390-396.

[4] C. L. Collins, "The kinematic analysis, design, and implementation of an in-parallel actuated telerobotic hand controller," Master's thesis, Mech. Aerosp. Eng., Univ. of California, Irvine, 1993.

[5] H. Iwata, "Artificial reality with force-feedback: Development of desktop virtual space with compact master manipulator," *Computer Graphics*, Vol. 24, no. 4, 1990, pp. 165-170.

[6] K. Woo, B. Jin, and D. Kwon, "A 6-DOF force-reflecting hand controller using the fivebar parallel mechanism," in *Proc. IEEE Int. Conf. Robotics and Automation*, 1998, pp. 1597-1602.

[7] J. Yoon and J. Ryu, "Design, fabrication and evaluation of a new haptic device using a parallel mechanism," Mobile Robots, vol. 6, no. 3, pp. 521-233, September 2001.

[8] C. L. Collins and G. L. Long, "The singularity analysis of an in-parallel hand controller for force-reflected teleoperation," *IEEE Trans. Robotics and Automation*, vol. 11, no. 5, October 1995, pp. 661-669.

[9] I. A. Bonev and J. Ryu, "A new approach to orientation workspace analysis of 6-DOF parallel manipulators," *Mechanism Mach. Theory*, vol. 36, pp.15-28.

[10]C. Gosselin, "Determination of the workspace of 6-dof parallel manipulators," *ASME J. Mech. Des.*, vol. 112, September 1990, pp. 331-336.

[11]T. H. Massie, J. K. Salisbury, "The PHANToM haptic interface: A device for probing virtual objects," ASME Winter Annual Meeting, DSC-vol. 55-1, November 1994, pp. 295-300.

[12]V. Hayward et al., "Freedom-7: A high fidelity seven-axis haptic device with application to surgical training," in Experimental robotics V, A. Casals and A. T. de Almeida, Eds. New York: Springer, 1998, vol. 232, Lecture Notes in Control and Information Science, pp. 445-456.

[13]K. H. Hunt, "Structural kinematics of in-parallel-actuated robot arms," *Trans. ASME: J. Mechanisms, Transmissions, and Automation in Design*, vol. 105, 1983, pp. 705-712.

[14]K. J. Waldron and K. H. Hunt, "Series-parallel dualities in actively coordinated mechanisms," in *Proc. Robotics Research: The Fourth Int. Symp.*, 1987, pp. 233-239.